Ion Jets Within Current Sheets in the Martian Magnetosphere

Y. Harada, J. Halekas, S. Xu, G. Dibraccio, S. Ruhunusiri, T. Hara, J. Mcfadden, J. Espley, D. Mitchell, C. Mazelle

JGR Space Physics

RESEARCH ARTICLE
10.1029/2020JA028576

Ion Jets Within Current Sheets in the Martian Magnetosphere

Y. Harada[1], J. S. Halekas[2], S. Xu[3], G. A. DiBraccio[4], S. Ruhunusiri[2], T. Hara[3], J. P. Mcfadden[3], J. R. Espley[4], D. L. Mitchell[3], and C. Mazelle[5]

[1]Department of Geophysics, Kyoto University, Kyoto, Japan, [2]Department of Physics and Astronomy, University of Iowa, Iowa City, IA, USA, [3]Space Sciences Laboratory, University of California, Berkeley, CA, USA, [4]NASA Goddard Space Flight Center, Greenbelt, MD, USA, [5]IRAP, University of Toulouse, CNRS, UPS, CNES, Toulouse, France

Key Points:
- Both sunward and anti-sunward ion jets embedded within current sheets are widely and commonly observed in the near Mars space
- Magnetic field configuration and topology around the jets are generally consistent with those expected from magnetic reconnection
- The jet occurrence appears independent of upstream drivers, possibly resulting from ubiquitous formation of low-beta, thin current sheets

Correspondence to:
Y. Harada,
haraday@kugi.kyoto-u.ac.jp

Citation:
Harada, Y., Halekas, J. S., Xu, S., DiBraccio, G. A., Ruhunusiri, S., Hara, T., et al. (2020). Ion jets within current sheets in the Martian magnetosphere. *Journal of Geophysical Research: Space Physics*, *125*, e2020JA028576. https://doi.org/10.1029/2020JA028576

Received 12 AUG 2020
Accepted 23 OCT 2020
Accepted article online 11 NOV 2020

Abstract Magnetic reconnection is often suggested to be implicated in a variety of dynamic phenomena observed in the complex magnetosphere of Mars. We present a first global survey of ion jets within current sheets, which are thought of as a primary product of magnetic reconnection, with Mars Atmosphere and Volatile EvolutioN (MAVEN) data obtained on the dayside and nightside in the Martian magnetosphere. We develop a fully automated algorithm to efficiently and reliably identify ion flow velocity deviations during current sheet crossings recorded by MAVEN. The obtained statistical results show that (i) sunward and anti-sunward ion jets embedded within current sheets are commonly and widely observed in the dayside and nightside magnetosphere of Mars, (ii) measured magnetic field profiles and inferred magnetic topology during the jet crossings are generally consistent with those expected for reconnecting current sheets, (iii) the jet occurrence is apparently independent of upstream driver conditions, and (iv) most of the identified current sheets are thin with a roughly ion scale half-thickness and are embedded in low beta plasma, suggesting that they are seemingly capable of reconnection based on the known onset conditions. The widespread distributions and common detection of ion jets, as well as the ubiquitous presence of thin, low-beta current sheets, imply that magnetic reconnection could operate frequently in many locations around Mars, thereby playing an important role in the dynamics of the Martian magnetosphere for most, if not all, of the solar wind conditions in the present epoch.

1. Introduction

The solar wind interaction with the upper atmosphere and crustal magnetic fields of Mars leads to the formation of a complex magnetosphere in which both induced and planetary (crustal) magnetic fields play a role (DiBraccio et al., 2018; Dubinin & Fraenz, 2015; Nagy et al., 2004; Xu et al., 2020). As the Martian magnetosphere shapes pathways of the energy input from the solar wind to the atmosphere and of escaping ions from the atmosphere to space, understanding the structure and dynamics of this region is vitally important if we are to fully comprehend the solar-Martian system and its impact on the atmospheric evolution of Mars. Since the arrival to Mars in 2014, the Mars Atmosphere and Volatile EvolutioN (MAVEN) mission (Jakosky et al., 2015) has been providing a wealth of information on the Martian magnetosphere with its comprehensive plasma and fields instrumentation and with its orbital coverage of relevant interaction regions including the solar wind, magnetosheath, magnetosphere, and ionosphere around Mars.

Among a number of physical processes potentially controlling the plasma dynamics in the Martian magnetosphere (e.g., Dubinin et al., 2012), magnetic reconnection is often suggested to be directly or indirectly implicated in producing many observed phenomena such as magnetic flux ropes (Brain et al., 2010; Beharrell & Wild, 2012; DiBraccio et al., 2015; Hara et al., 2014, 2016, 2017; Soobiah et al., 2014), acceleration of auroral electrons (Brain et al., 2006; Brain & Halekas, 2013; Xu et al., 2020), trapping of electrons on closed field lines (Brain et al., 2007; Harada et al., 2016; Xu et al., 2017), bursty particle fluxes (Dubinin et al., 2012), transient ionospheric structures (Kopf et al., 2008, 2017), and the twisted magnetotail (DiBraccio et al., 2018). It is proposed that a variety of current sheet configurations capable of reconnection are possible because of the interplay between the draped interplanetary magnetic field (IMF) and crustal magnetic fields of Mars (Halekas & Brain, 2010; Krymskii et al., 2002), leading to a speculation that magnetic reconnection might operate commonly in many locations around Mars. Before MAVEN, electron and magnetic signatures indicative of reconnection occurrence were identified (Eastwood et al., 2008; Halekas et al., 2009), but the

lack of adequate instrumentation prohibited comprehensive investigation of in situ reconnection signatures (Paschmann et al., 2013) with a complete set of ion, electron, and magnetic field data.

After the arrival of MAVEN, in situ signatures of collisionless magnetic reconnection were investigated in the nightside magnetotail of Mars on a case basis (Harada et al., 2015b) and on a statistical basis (Harada et al., 2017). The newly identified in situ reconnection signatures at Mars include ion jets embedded within current sheets, which are often thought of as one of the primary measurable products of magnetic reconnection (e.g., Paschmann et al., 1979, 2013). Prompted by a recent finding of a case with similar reconnection signatures on the dayside of Mars (Harada et al., 2018) and by recently suggested global consequences of dayside reconnection (DiBraccio et al., 2018), we conduct a further statistical survey of reconnection signatures with a wider spatial coverage including the dayside magnetosphere. Here we highlight important updates in this paper from the previous work by Harada et al. (2017). First, to statistically characterize near Mars magnetic reconnection signatures on both the dayside and nightside, we extend the search region previously limited to the central magnetotail (i.e., the geometrical shadow Harada et al., 2017) to the entire magnetosphere below the induced magnetospheric boundary. Second, in contrast to Harada et al. (2017), who searched for Hall magnetic field signatures first following the methodology originally developed for Mars Global Surveyor (MGS) data (Halekas et al., 2009), we primarily identify accelerated ion flows embedded within current sheets (i.e., ion jets) to better capture the ion dynamics potentially driven by magnetic reconnection. Third, we develop a fully automated algorithm that identifies the ion jets detected during current sheet crossings to efficiently utilize the increasing data volume accumulated by MAVEN. The obtained statistical results provide a first-ever global view as to when and where these reconnection signatures are observed within the Martian magnetosphere.

2. Data

We utilize particles and fields data obtained by MAVEN from 1 December 2014 to 31 December 2019 (roughly 10,000 orbits in total). We analyze magnetic field data from the magnetometer (MAG; Connerney et al., 2015), ion data from the SupraThermal and Thermal Ion Composition (STATIC) instrument (McFadden et al., 2015), electron data from the Solar Wind Electron Analyzer (SWEA; Mitchell et al., 2016), and upstream solar wind data from the Solar Wind Ion Analyzer (SWIA; Halekas et al., 2015). To resolve ion velocity variation during a quick current sheet crossing, we compute ion velocity moments from high time resolution (4 s), four-dimensional (resolved in energy, azimuthal angle, elevation angle, and mass) STATIC "d1" data products (see McFadden et al., 2015) corrected for the potential and velocity of the spacecraft by using publicly available software (Angelopoulos et al., 2019). We also use magnetic topology data inferred from electron distributions (Xu et al., 2019).

3. Methodology

In this section, we describe an automated procedure to identify (sub-)Alfvénic ion jets embedded within current sheets from MAVEN data.

First we identify current sheet crossings in the Martian magnetosphere. We utilize a slightly modified version of the previously developed procedures to search for a relatively quick magnetic field rotation recorded by a traveling spacecraft (Halekas & Brain, 2010; Harada et al., 2017). Using 1-s resolution MAG data, we derive average magnetic field vectors on the precrossing (hereafter denoted by a subscript "1") and postcrossing ("2") sides, $\mathbf{B}_1$ from -150 s $< t < -45$ s and $\mathbf{B}_2$ from $+45$ s $< t < +150$ s, respectively. We compute the dot product of their normalized vectors, $\mathbf{b}_1 \cdot \mathbf{b}_2$, and flag the center time ($t = 0$) as a tentative current sheet crossing if $\mathbf{b}_1 \cdot \mathbf{b}_2 < 0$ (corresponding to >90° rotation). In contrast to the previous studies by Halekas and Brain (2010) and Harada et al. (2017), we do not require a field magnitude depression during the crossing to include current sheets with no apparent dip in $|\mathbf{B}|$ that are known to be present in the near Mars space (Artemyev et al., 2017). Of the tentatively identified current sheet crossings, we reject a crossing if (i) $|\mathbf{B}_1|$<5 nT or $|\mathbf{B}_2|$<5 nT to exclude rapid magnetic field fluctuations often present in a weak field plasma, (ii) the induced-to-total field ratio, $|\mathbf{B} - \mathbf{B}_c|/|\mathbf{B}|$, where $\mathbf{B}_c$ is the local crustal magnetic field computed from the spherical harmonic model by Langlais et al. (2019), is below 0.8 on either side to eliminate magnetic field variation attributed purely to crustal fields, (iii) the ratio of proton to heavy (O^+ plus O_2^+) ion number densities exceeds unity during the crossing, thereby focusing on current sheets located below the induced magnetospheric boundary (for which we take the ion composition boundary, but see also Xu et al. (2016),

Matsunaga et al. (2017), Espley (2018), and Halekas et al. (2018) for differences in differently defined boundaries), (iv) the crossing is observed below a 200 km altitude to focus on collisionless plasma, and (v) the 4-s ion velocity data are not available. From the MAVEN data described in section 2, we identified 6497 potential current sheet crossings.

Next, we utilize the minimum variance analysis (MVA; Sonnerup & Cahill, 1967) of magnetic fields to infer the local structure of each current sheet. Our primary aim here is to determine the current sheet orientation and to define the precrossing "lobe" region, central current sheet region, and postcrossing "lobe" region for each current sheet so that we can identify accelerated ion flows within current sheets in an automated fashion. As a first step, we apply MVA to magnetic field data with a fixed time window from -150 s $< t < +150$ s of each crossing to provide an initial estimate of the current sheet *LMN* coordinate system, in which *L* is along the anti-parallel magnetic field components (i.e., the maximum variance direction), *M* is along the guide field direction (intermediate variance direction), and *N* is along the current sheet normal direction (minimum variance direction). In this paper, we choose the polarity of the *LMN* system so that *L* has a sunward ($+X_{\mathrm{MSO}}$) component and *N* points toward the spacecraft velocity direction ($+V_{\mathrm{SC}}$). We then fit the observed B_{L} to a Harris sheet field, $B_{\mathrm{L}} = -B_{\mathrm{L,1,Harris}} \tanh((t - t_{\mathrm{c,Harris}})/W_{\mathrm{Harris}})$ to estimate the crossing time duration, which is variable from crossing to crossing. By using the estimated crossing duration, we re-apply MVA to the magnetic field data from $t_{\mathrm{c,\,Harris}} - 2W_{\mathrm{Harris}} < t < t_{\mathrm{c,\,Harris}} + 2W_{\mathrm{Harris}}$, thereby updating the initial *LMN* system to a new one derived from the adaptively chosen data segment of each crossing. We re-fit the updated B_{L} to a Harris field and obtain a new set of parameters, $B_{\mathrm{L,\,1,\,Harris}}$, $t_{\mathrm{c,\,Harris}}$, and W_{Harris}, which will be used in the following analysis. We filter out current sheets if the maximum-to-intermediate eigenvalue ratio, $\lambda_{\mathrm{L}}/\lambda_{\mathrm{M}}$, is below 4 to eliminate events with ill-defined *L* direction or if the correlation coefficient between the observed and fitted B_{L} profiles, R_{Harris}, is below 0.95 to eliminate complex B_{L} profiles such as those including multiple partial crossings within a full crossing (e.g., DiBraccio et al., 2015, 2017). The R_{Harris} threshold of 0.95 is chosen such that a small deviation from a Harris sheet (e.g., bifurcated current sheets and thin, inner current sheets; Grigorenko et al., 2019; Harada et al., 2018) is accepted yet reliable automatic detection of ion jets is feasible. As a result, we selected 3,163 current sheets with relatively clean B_{L} profiles.

Finally, we identify ion flows accelerated along the *L* direction within current sheets (hereafter called ion $\pm V_{\mathrm{L}}$ jets with signs denoting whether the jet is directed sunward/anti-sunward). To investigate plasma acceleration within current sheets, we use an ion mass flow velocity computed from the average of H^+, O^+, and O_2^+ ion velocities weighted by their mass densities. We note that as momentum transfer from the solar wind to the ionospheric plasma will nominally produce anti-sunward mass flows (e.g., Lundin, 2011), the generation of a sunward mass flow requires an additional process such as magnetic reconnection. We will explore alternative explanations for the observed "jets" in the discussion section. We select ion + (−) V_{L} jet events based on three criteria using the ion V_{L} component in the precrossing ($t_{\mathrm{c,\,Harris}} - 2W_{\mathrm{Harris}} < t < t_{\mathrm{c,\,Harris}} - W_{\mathrm{Harris}}$), central current sheet ($t_{\mathrm{c,\,Harris}} - W_{\mathrm{Harris}} < t < t_{\mathrm{c,\,Harris}} + W_{\mathrm{Harris}}$), and postcrossing ($t_{\mathrm{c,\,Harris}} + W_{\mathrm{Harris}} < t < t_{\mathrm{c,\,Harris}} + 2W_{\mathrm{Harris}}$) regions: (i) a positive (negative) peak of the V_{L} profile in the central current sheet region should deviate from the mean V_{L} in the precrossing and postcrossing regions by more than 2 standard deviations; (ii) the peak value of V_{L} should be positive (negative) in the Mars rest frame; and (iii) the upper (lower) quartiles of V_{L} in the central current sheet region should deviate from the mean V_{L} in the precrossing and postcrossing regions by more than 0.1 V_{A}, where V_{A} is the Alfvén velocity in the corresponding regions. The criterion (i) ensures that the observed peak in the current sheet is well above the fluctuations in the precrossing and postcrossing regions. We impose the criterion (ii) to eliminate apparent deceleration of anti-sunward flows caused by an ion beam moving out of the instrument field of view by requiring that $+V_{\mathrm{L}}$ jets do flow sunward with respect to Mars, while it has no practical effect on identification of $-V_{\mathrm{L}}$ jets. The criterion (iii) ensures that the ion jet is not much slower than the expected plasma acceleration by magnetic reconnection. Out of the 3,163 clean current sheet crossings, we identified 179 $+V_{\mathrm{L}}$ jet events and 179 $-V_{\mathrm{L}}$ jet events.

4. Case Studies

This section presents representative cases of the identified ion jet events to demonstrate the aforementioned data and methodology.

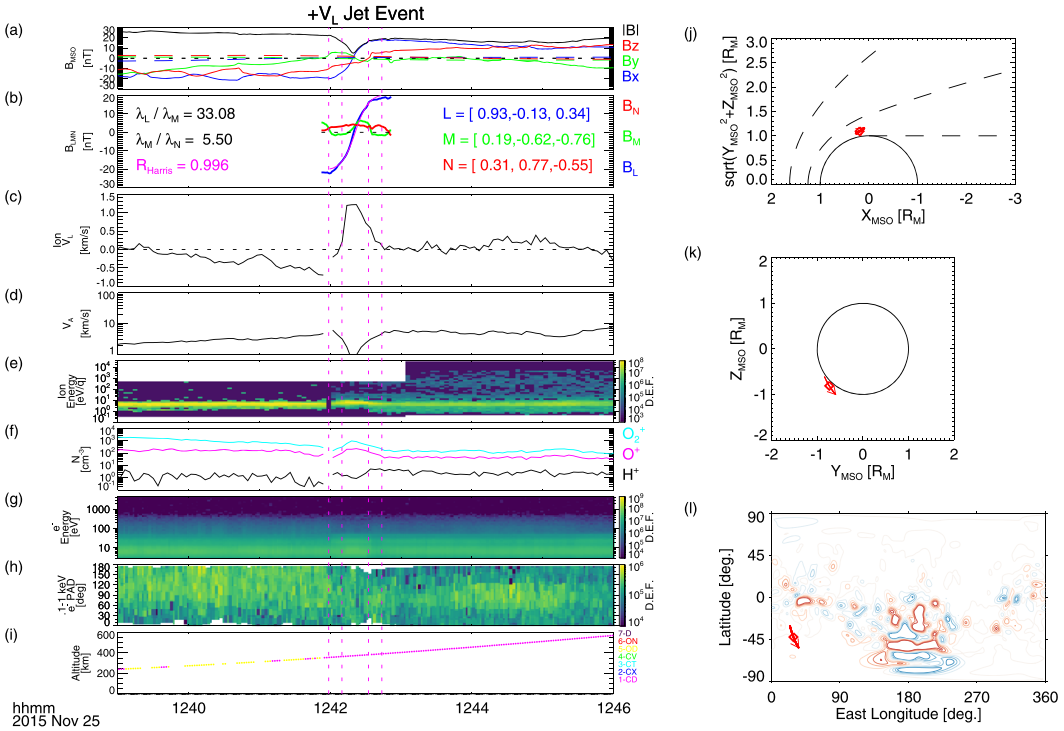

Figure 1. MAVEN observations at 12:39–12:46 UT on 25 November 2015 of (a) magnetic field in Mars Solar Orbital (MSO) coordinates with dashed lines denoting crustal field components computed from the spherical harmonic model by Langlais et al. (2019), (b) magnetic field in the *LMN* system (see text for details), (c) *L* component of the ion mass flow velocity, (d) Alfvén velocity, (e) ion energy spectra in units of differential energy flux (D.E.F.) of eV/cm^2/s/sr/eV, (f) ion densities, (g) electron energy spectra, (h) pitch angle distributions of 100 eV–1 keV electrons, (i) spacecraft altitude, and spacecraft trajectories (j) in cylindrical MSO coordinates (k) on the Y_{MSO}-Z_{MSO} plane, and (l) in geographic coordinates. In Figure 1b, the results of the minimum variance analysis are denoted and the Harris sheet fit is shown by the magenta curve. The altitude in Figure 1i is color coded by magnetic topology inferred from electron distributions (Xu et al., 2019): CD (magenta) = closed-to-day; CX (blue) = cross-terminator-closed; CT (cyan) = closed-trapped; CV (green) = voids; OD (yellow) = open-to-day; ON (red) = open-to-night; D (black) = draped. The dashed lines in Figure 1i show the nominal locations of the bow shock and magnetic pileup boundary from Trotignon et al. (2006) and the geometric shadow boundary. The contours in Figure 1l show the radial component (red = outward; blue = inward) of crustal magnetic fields at 400 km altitude.

4.1. A Sunward Ion Jet Event

Figure 1 shows a $+V_L$ jet event observed on 25 November 2015. MAVEN was located on the dayside near the terminator (Figure 1j), on the dawn side (Figure 1k), and over mostly unmagnetized regions (Figure 1l). We observe a B_x reversal around 12:42:21 UT (Figure 1a) representing a current sheet crossing and the corresponding B_L profile is well fitted by a Harris field (Figure 1b). The vertical magenta lines show the times at $t_{c,\,Harris} - 2W_{Harris}$, $t_{c,\,Harris} - W_{Harris}$, $t_{c,\,Harris} + W_{Harris}$, and $t_{c,\,Harris} + 2W_{Harris}$, defining the precrossing, central current sheet, and postcrossing regions. In the central current sheet region, the ion V_L deviates toward the positive *L* direction from the surrounding values in the precrossing and postcrossing regions (Figure 1c), indicating the presence of a sunward ion jets within the current sheet. The observed V_L deviation of ~1 km/s is only a fraction of V_A in the surrounding regions (Figure 1d), which is consistent with the previously reported reconnection jet events at Mars (Harada et al., 2015b, 2017, 2018) and simulation results (Ma et al., 2018). The incomplete acceleration at the observed location presumably results from relatively large scale lengths of heavy ions that can be comparable to sizes of magnetospheric structures at Mars (e.g., Ma et al., 2018), implying that the ions are not fully coupled to the magnetic field. Throughout the presented time interval, cold ionospheric ions are observed (Figures 1e and 1f). In Figure 1i, the spacecraft altitude is color coded by categories of inferred magnetic topology according to Xu et al. (2019). We generally observe "open-to-day" topology (yellow dots in Figure 1i) as inferred from the parallel photoelectrons and anti-parallel solar wind electrons before 12:42 UT, while "closed-to-day" topology (magenta dots

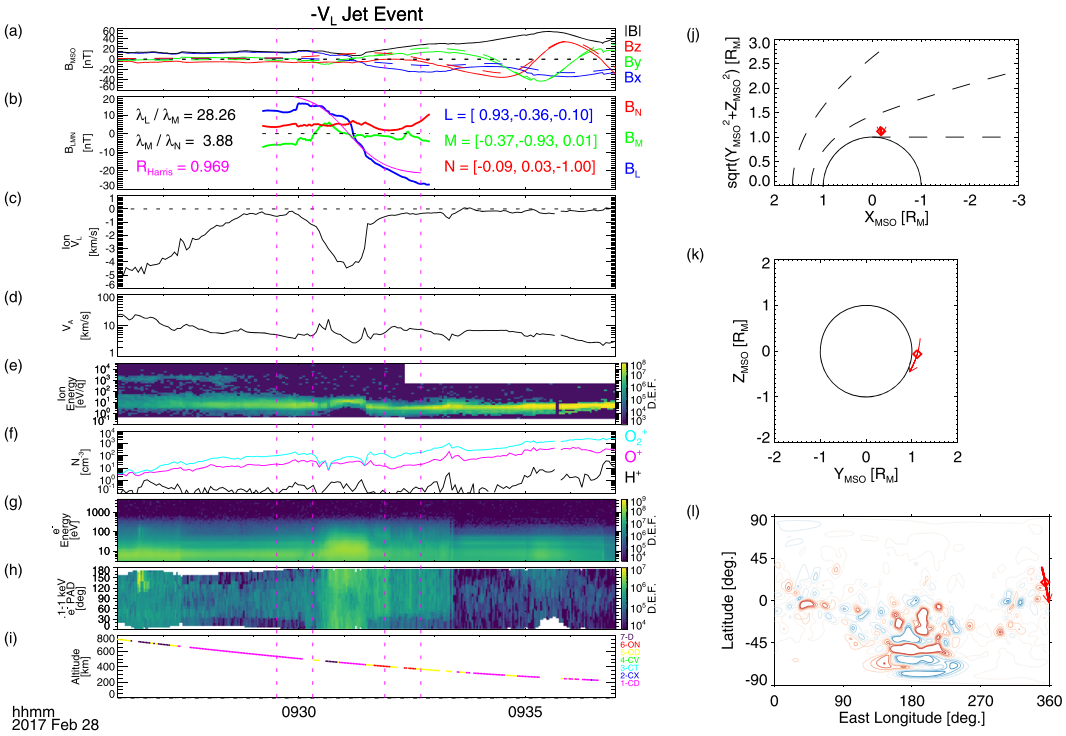

Figure 2. MAVEN observations at 09:26–09:37 UT on 28 February 2017 in the same format as Figure 1.

in Figure 1i) is observed after that as inferred from parallel and anti-parallel electrons both dominated by ionospheric photoelectrons (Figures 1g–1i).

4.2. An Anti-Sunward Ion Jet Event

Figure 2 shows a $-V_L$ jet event observed on 28 February 2017. MAVEN was located on the night side near the terminator (Figure 2j), on the dusk side (Figure 2k), and near moderately strong crustal magnetic fields (Figure 2l). A B_x reversal was recorded around 09:31:06 UT, followed by smooth magnetic field variations consistent with crustal fields (Figure 2a). The B_L profile (Figure 2b) is not as clean as that shown in Figure 1b, but the Harris sheet field still provides a reasonable fit with $R_{Harris} \sim 0.97$. We observe a clear deviation of ion V_L toward the negative L direction in the central current sheet region (Figure 2c), indicating anti-sunward ion acceleration within the current sheet. The observed V_L deviation of ~ -4.5 km/s is comparable to $V_A \sim 5$ km/s in the precrossing region and somewhat smaller than $V_A \sim 8$ km/s in the postcrossing region (Figure 2d). The observed ions display characteristics of ionospheric origin (Figures 2e and 2f). The electron distributions (Figures 2g–2i) imply the "closed-to-day" topology in the precrossing region, a mixture of various topological categories ("open-to-day," "draped," "closed-to-day," and "open-to-night") in the central current sheet region, and "open-to-day" or "open-to-night" topology in the postcrossing region.

5. Statistical Properties

We now investigate statistical properties of the identified ion $\pm V_L$ jets.

5.1. Spatial Distributions

Figure 3a shows the observed locations of the relatively clean ($R_{Harris} > 0.95$ and $\lambda_L/\lambda_M > 4$) current sheet crossings and $\pm V_L$ jets as a function of altitude and solar zenith angle (SZA). Because of the ion composition requirement (dominance of heavy ions over protons), most of the identified current sheets are confined below the nominal magnetic pileup boundary (MPB; Trotignon et al., 2006). Both of the $\pm V_L$ jets are widely distributed in the Martian magnetosphere, though the sunward $+V_L$ (anti-sunward $-V_L$) jets tend to be observed more frequently on the day (night) side. The symbol size represents the magnitude of peak V_L deviation normalized by V_A averaged from the precrossing and postcrossing regions. The observed V_L jets are typically sub-Alfvénic with V_L deviation of only a fraction of V_A, suggesting incomplete acceleration

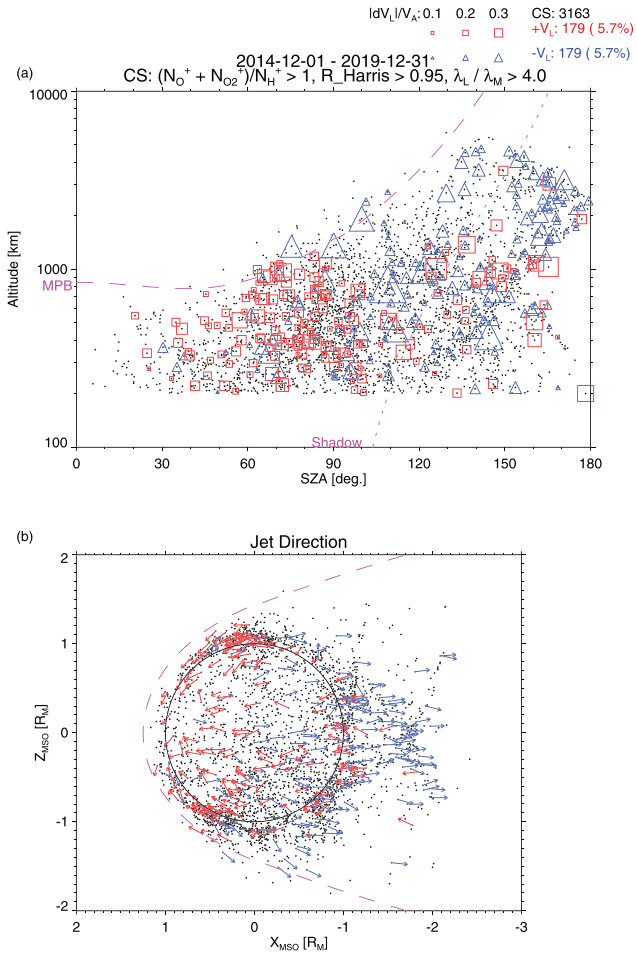

Figure 3. (a) Altitude-solar zenith angle (SZA) distributions of the relatively clean current sheets (black dots), $+V_L$ ion jets (red squares), and $-V_L$ ion jets (blue triangles). The symbol size represents $\Delta V_L/V_A$ averaged from the two sides of each jet event. The magenta dashed line shows the nominal location of the magnetic pileup boundary (MPB) from Trotignon et al. (2006). The magenta dotted line denotes the geometric shadow boundary. (b) Z_{MSO}-X_{MSO} distributions of the relatively clean current sheets (black dots), $+V_L$ ion jets (red arrows), and $-V_L$ ion jets (blue arrows). The arrows show the projections of the $\pm L$ direction with polarities corresponding to the ion jet directions. The magenta dashed line denotes the nominal MPB on the X_{MSO}-Z_{MSO} plane.

of ion flows and partial decoupling of ions from the reconnected field lines as proposed by the previous results (Harada et al., 2015b, 2017, 2018; Liu et al., 2015; Ma et al., 2018). In Figure 3b, the jet directions ($\pm L$ directions) are projected on the X_{MSO}-Z_{MSO} plane. It can be seen that most of the jets are aligned with the expected IMF draping configuration (mostly horizontal on the dayside and aligned with the Sun-Mars line in the nightside magnetotail Crider et al., 2004), suggesting that the draped IMF is implicated in the formation of these current sheets, as inferred from previous MGS results (Halekas & Brain, 2010; Halekas et al., 2009). The mixture of sunward and anti-sunward jets over a wide range of SZAs suggests that at a given time the X-line could be present almost anywhere (in terms of MSO coordinates) in the near Mars magnetosphere.

Next we display geographic distributions of the identified current sheets and $\pm V_L$ jets in Figure 4. Both on the dayside (Figure 4a) and nightside (Figure 4b), the current sheets (black dots) are distributed over wide areas of geographic coordinates, indicating ubiquitous formation of current sheets around the planet. Meanwhile, the ion jet locations (red squares and blue triangles) in Figure 4 exhibit some clustering around the magnetized areas. This clustering could result from some favorable conditions of ion jet generation near the strong crustal fields and/or it may be attributed to higher detectability of ion jets in current sheets with stronger magnetic fields (a higher absolute jet speed caused by higher V_A implies easier detection of the V_L deviation from artificial and natural fluctuations in ion velocity data). We note that many of the jets are

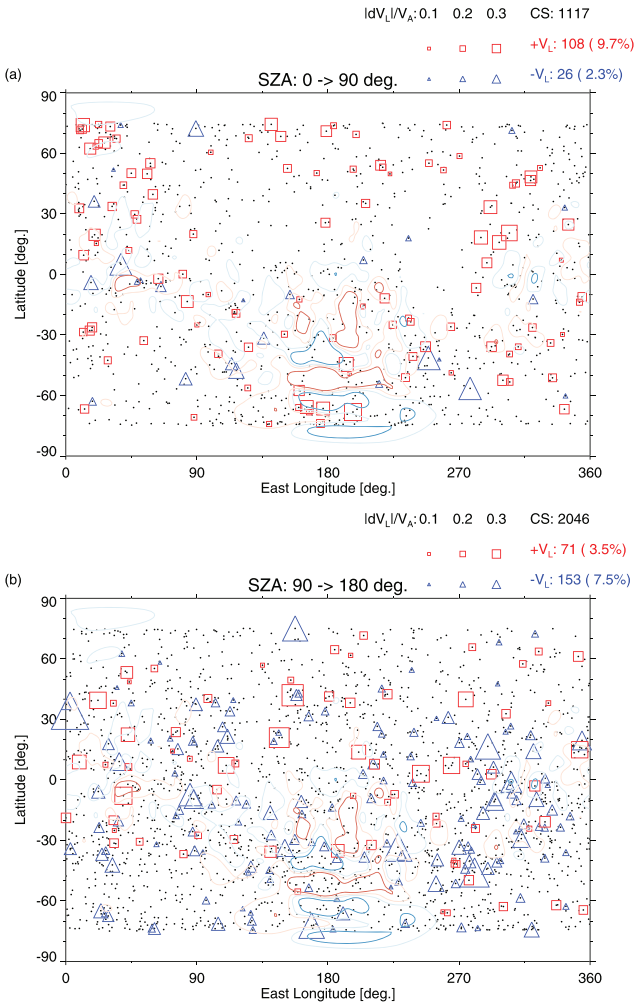

Figure 4. Geographic distributions of the relatively clean current sheets (black dots), $+V_L$ ion jets (red squares), and $-V_L$ ion jets (blue triangles) observed (a) on the dayside and (b) on the nightside. The contours in Figures 4a and 4b show the radial component (red = outward; blue = inward) of crustal magnetic fields at 400 km altitude.

observed above the weakly magnetized and unmagnetized areas, suggesting that the jets can be generated within current sheets of noncrustal field origin.

5.2. Magnetic Field Configuration and Topology

We now look at averaged magnetic structures separately for the sunward and anti-sunward jet events. Figure 5 illustrates the expected field and velocity variations (Figure 5b) for a spacecraft crossing the $+/-L$ sides of the X-line (Figure 5a). The quadrupolar out-of-plane Hall magnetic field (Eastwood et al., 2008; Halekas et al., 2009; Nagai et al., 2001; Øieroset et al., 2001; Pritchett, 2001; Yamada et al., 2010) will be observed as a negative-to-positive (positive-to-negative) bipolar B_M variation for the $+V_L$ ($-V_L$) jets regardless of the $B_{L,1}$ polarity, provided that the polarity of N is chosen correctly. Meanwhile, the normal field associated with reconnection will emerge as a negative (positive) offset in B_N for the $+V_L$ ($-V_L$) jets if $B_{L,1} > 0$, and as an offset opposite to it if $B_{L,1} < 0$. Combining these profiles, the $+V_L$ ($-V_L$) jets will be accompanied by a negative-to-positive (positive-to-negative) bipolar $B_M/|B_{L,1}|$ variation and a negative (positive) $B_N/B_{L,1}$ offset (Figure 5c) during a crossing of a reconnecting current sheet.

We test this prediction using the observed magnetic field profiles during the jet detection in Figure 6. Figures 6a and 6b show superposed epoch analysis results of normalized magnetic fields, $B_L/B_{L,1,\mathrm{Harris}}$, $B_M/|B_{L,1,\mathrm{Harris}}|$, and $B_N/B_{L,1,\mathrm{Harris}}$, as a function of relative crossing time, $(t-t_{c,\mathrm{Harris}})/W_{\mathrm{Harris}}$ for the identified $+V_L$ and $-V_L$ jet events, respectively. For reference, the corresponding V_L/V_A profiles are shown in Figures 6c and 6d. For the $+V_L$ jets (Figures 6a and 6c), the negative-to-positive variation in $B_M/|B_{L,1,\mathrm{Harris}}|$

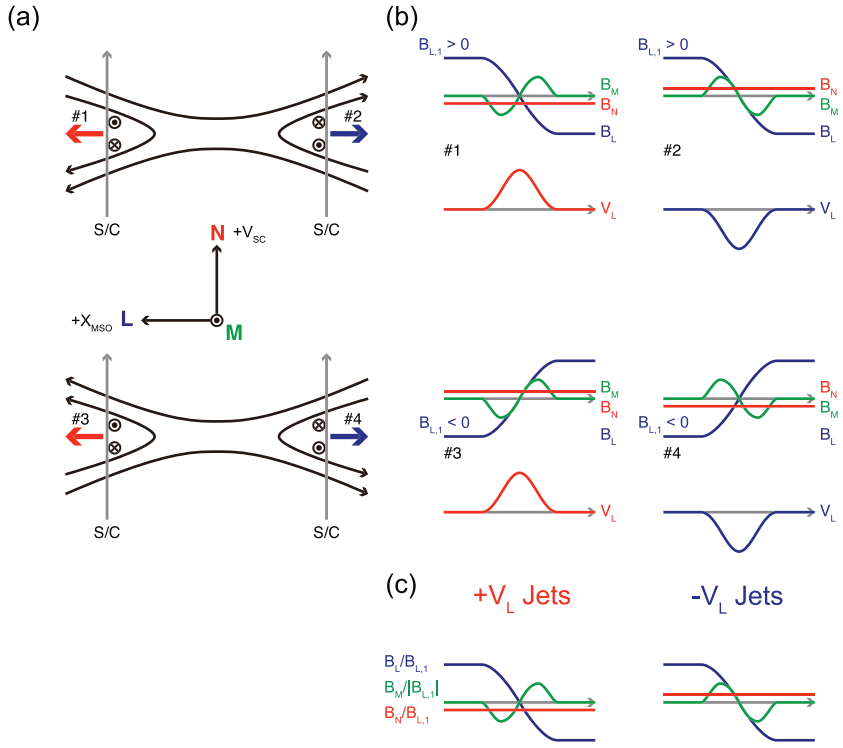

Figure 5. Expected magnetic field and ion V_L variations observed by a spacecraft crossing a reconnecting current sheet.

(green) and the negative offset in $B_N/B_{L,1,Harris}$ (red) are observed along with the $+V_L$ deviation. Conversely, for the $-V_L$ jets (Figures 6b and 6d), the positive-to-negative variation in $B_M/|B_{L,1,Harris}|$ (green) and the positive offset in $B_N/B_{L,1,Harris}$ (red) are observed along with the $-V_L$ deviation. Note that these signatures do not appear if we take averages from the overall crossings (dashed lines). This demonstrates that we indeed observe the expected magnetic field configuration during spacecraft crossings of reconnecting current sheets.

Energy and pitch angle distributions of suprathermal electrons have proven useful to infer magnetic topology around Mars (Brain et al., 2007; Weber et al., 2017, 2019; Xu, Mitchell, Liemohn, et al., 2017; Xu, Mitchell, Luhmann, et al., 2017; Xu et al., 2018, 2019), which can be altered by magnetic reconnection. Figures 6e and 6f show average energy spectra during crossings of the $+V_L$ and $-V_L$ jets, respectively. Here the observed energy and differential energy flux (uncorrected for spacecraft charging) are used for straightforwardness of averaging and only >10 eV energies are shown, as the spacecraft potential is typically small (<+10 V) below the magnetosheath. On average, we observe cold energy spectra typical of ionospheric photoelectrons throughout the $+V_L$ jet crossing (Figure 6e) with a slight flux decrease above ~200 eV around the crossing center. Meanwhile, a clear enhancement of electron flux is seen around the center of the $-V_L$ jet crossing (Figure 6f), which is reminiscent of similar MGS measurements of electron flux enhancement postulated as a consequence of reconnection between draped IMF and crustal fields (Uluşen & Linscott, 2008). We note that the majority of the $+V_L$ ($-V_L$) jets are observed on the dayside (nightside) as shown in Figure 3, possibly providing an explanation for the difference between off-center (background) energy spectra of $+V_L$ and $-V_L$ jet crossings, but reasons for the difference in variations of energy spectra do not seem immediately obvious. Figures 6g and 6h show distributions of magnetic topology categories inferred by Xu et al. (2019)'s method from electron energy and pitch angle distributions. To display the variations of categorical data as a function of relative crossing time, we count the number of each topology category nearest to the superposed epoch bin (thus one crossing event contributes one count in each epoch bin) and show this series of histograms in a spectrogram format. On one hand, Figure 6g indicates that closed-to-day (labeled "C-D") is the dominant category throughout the $+V_L$ jet crossing as expected from the photoelectron-dominated average spectra (Figure 6e), but the open-to-day ("O-D"), open-to-night ("O-N"), and draped ("DP") categories are increasingly populated in the precrossing and postcrossing regions instead of C-D. This implies that the

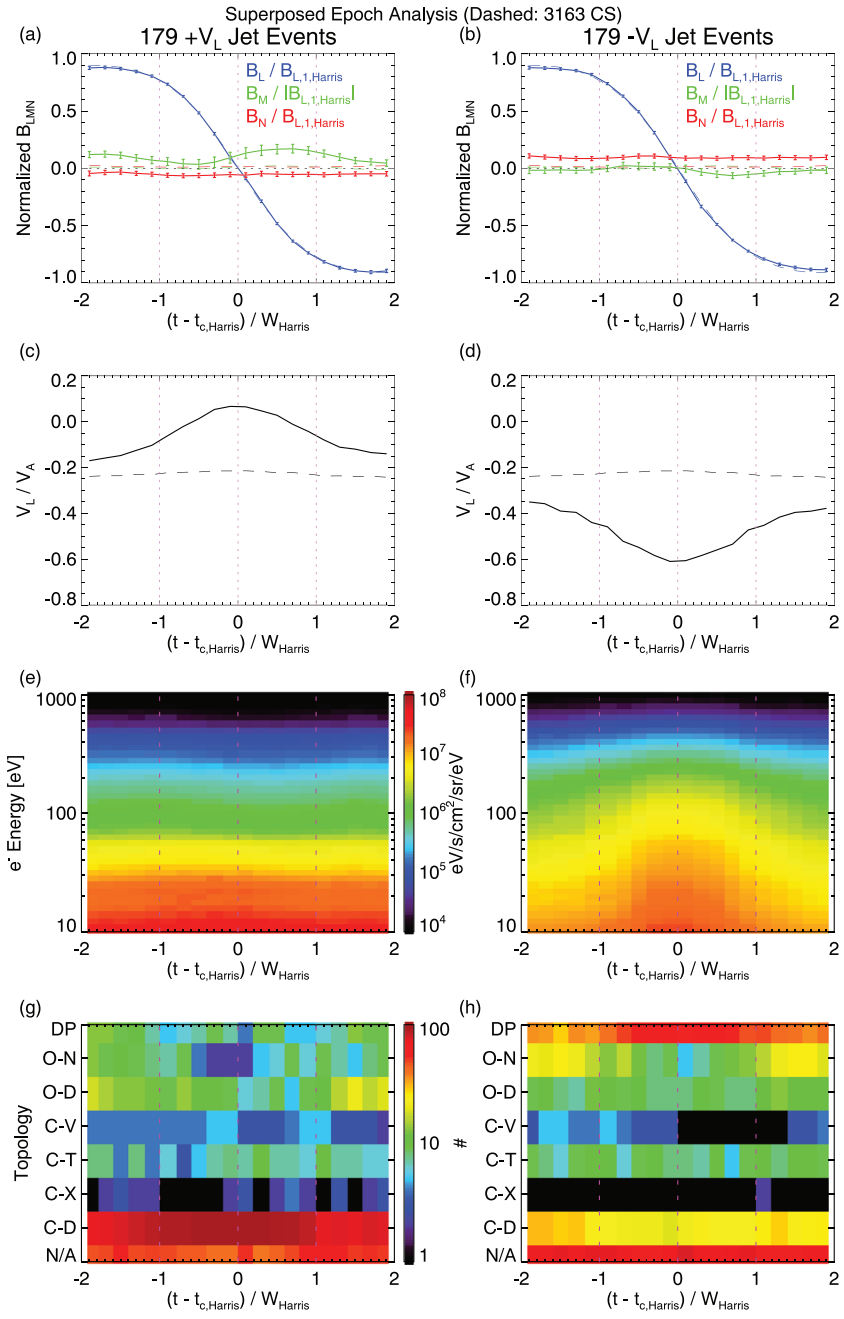

Figure 6. Superposed epoch analysis results of (left) $+V_L$ jet events and (right) $-V_L$ jet events. (a and b) Normalized B_L, B_M, and B_N profiles. The error bars represent 1 standard error of the mean. Note that B_M is normalized by unsigned $B_{L,1,Harris}$. (c and d) Ion V_L/V_A profiles, where V_A is the average of the precrossing and postcrossing regions of each event. (e and f) Electron energy spectra. The differential energy flux is averaged in a logarithmic manner. (g and h) Time series of histograms of magnetic topology categories inferred from electron distributions (Xu et al., 2019): N/A = not available; C-D = closed-to-day; C-X = cross-terminator-closed; C-T = closed-trapped; C-V = voids; O-D = open-to-day; O-N = open-to-night; and DP = draped. The dashed lines in Figures 6a–6d show the results for all the relatively clean current sheets.

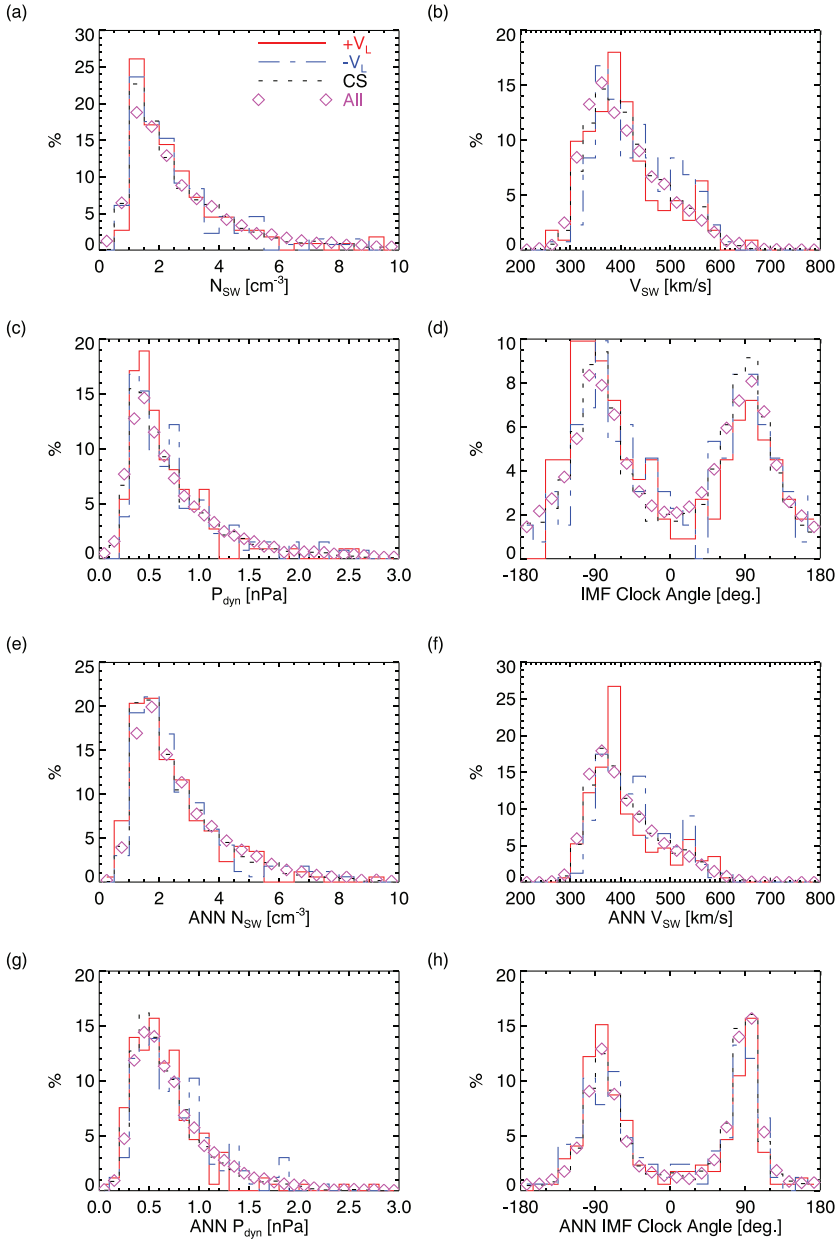

Figure 7. Normalized histograms of upstream drivers for the $+V_L$ jet events (red, solid lines), $-V_L$ jet events (blue, dash-dot lines), relatively clean current sheet crossings (black, dotted lines), and all data (magenta diamonds). (a–d) Direct measurements by SWIA and MAG (Halekas et al., 2016) and (e–h) artificial neural network (ANN) proxies derived by Ruhunusiri et al. (2018) of (a and e) solar wind density, (b and f) speed, (c and g) dynamic pressure, and (d and h) interplanetary magnetic field (IMF) clock angle.

closed topology is very likely to be seen concurrently with the $+V_L$ jets in the central current sheet, while more and more open and draped field lines are found as the spacecraft is located distant from the central current sheet. On the other hand, Figure 6h shows that the draped topology is the dominant type (among the identified topologies) around the center, while the O-N and C-D increase their presence in the precrossing and postcrossing regions. Taken together, the census of magnetic topology during crossings of the $\pm V_L$ jets suggests that the central $+V_L$ jets tend to be associated with the closed magnetic topology, which can be formed by the X-line located anti-sunward of the spacecraft, while the draped (detached) field lines are more likely to be seen for thecentral $-V_L$ jets as expected for the X-line located sunward of the spacecraft.

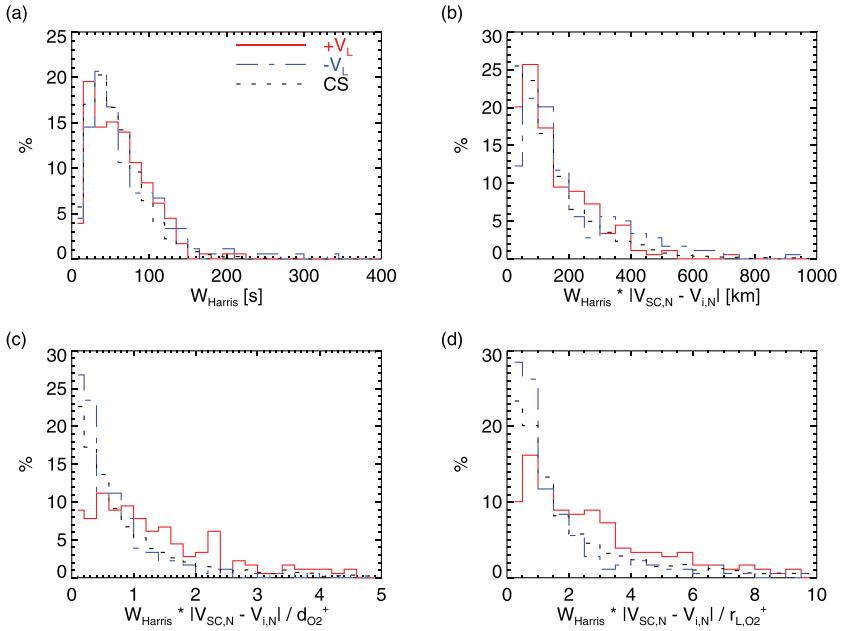

Figure 8. Normalized histograms of (a) current sheet crossing half-duration (W_{Harris}), (b) half-thickness ($W_{\mathrm{Harris}}|V_{\mathrm{SC,N}} - V_{\mathrm{i,N}}|$), and half-thickness normalized (c) by the O_2^+ ion inertial length and (d) by the O_2^+ ion thermal gyroradius, $r_{L,i} = m_i\sqrt{2T_i/m_i}/|qB_{\mathrm{L}}|$, where T_i is the average ion temperature in the central current sheet region and B_{L} is the lobe magnetic field strength (Runov et al., 2005; Vasko et al., 2014) for the $+V_{\mathrm{L}}$ jet events (red, solid lines), $-V_{\mathrm{L}}$ jet events (blue, dash-dot lines), and relatively clean current sheet crossings (black, dotted lines).

5.3. Dependences on Upstream Drivers

Here we investigate dependences of the jet occurrence on upstream solar wind conditions. Figure 7 shows histograms of upstream drivers for the identified jet events and current sheet crossings along with the overall distributions. In Figures 7a–7d, solar wind parameters directly measured by SWIA and MAG are shown, while artificial neural network (ANN) proxies derived by Ruhunusiri et al. (2018) are used in Figures 7e–7h. The ANN proxies have advantages that they can provide upstream driver estimates even for orbits with no direct solar wind measurements, while they could include some uncertainties because upstream conditions are inferred indirectly from magnetosheath measurements. We present both of these upstream driver data sets to ensure that observed trends (or lack thereof) do not arise from the biased coverage of direct solar wind measurements or from the uncertainties of ANN proxies. Among the investigated parameters, we show the solar wind density (Figures 7a and 7e), solar wind speed (Figures 7b and 7f), solar wind dynamic pressure (Figures 7c and 7g), and IMF clock angle (Figures 7d and 7h), which are often shown to have control of some aspects of the Martian magnetosphere (e.g., Dubinin et al., 2017; Ferguson et al., 2005; Harada et al., 2015a; Weber et al., 2019; Xu et al., 2018). Comparing the parameter histograms for the identified jet events, current sheets, and overall data, no obvious systematic differences are seen except for some fluctuations due to poor statistics. To date, we have not yet successfully identified any prominent dependence of the overall occurrence rate of ion jets on the driver parameters.

5.4. Current Sheet Thickness

Next we investigate local conditions which potentially control the occurrence of magnetic reconnection in current sheets. It is generally accepted that a current sheet must be sufficiently thin for reconnection to occur (e.g., Asano et al., 2003; Baumjohann et al., 2007; Paschmann et al., 2013). The current sheet thickness was previously estimated for cross-tail current sheets on the nightside of Mars (Grigorenko et al., 2017, 2019), demonstrating that ion scale, and even sub-ion scale, current sheets are commonly present in the Martian magnetotail. Here we conduct a similar analysis for the current sheets identified on the dayside and nightside of Mars. Figure 8 shows histograms of the current sheet half-thickness estimated from the Harris fit results for the identified $\pm V_{\mathrm{L}}$ jet events and relatively clean current sheet crossings. We obtain a rough estimate of current sheet half-thickness by multiplying the half-duration of crossing (Figure 8a) by the relative normal velocity of the spacecraft with respect to the ion mass flow (Figure 8b). It is seen that most of the

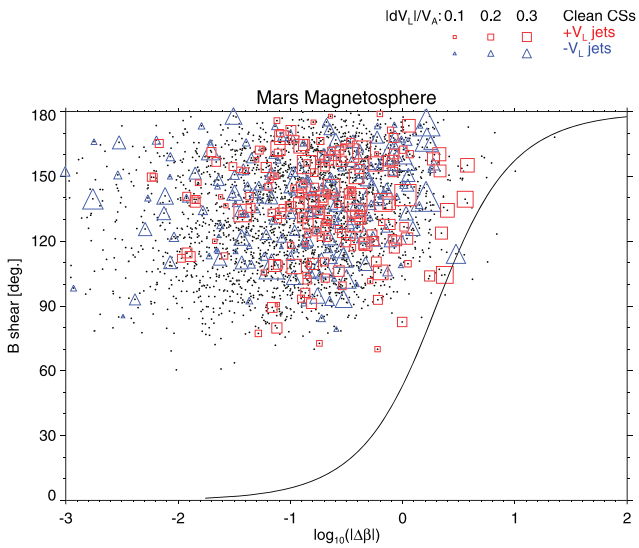

Figure 9. Scatter plots of magnetic shear and difference of plasma beta on the two sides of the current sheet for the $+V_L$ jet events (red squares), $-V_L$ jet events (blue triangles), and relatively clean current sheets (black dots) observed within the Martian magnetosphere. The solid curve marks a predicted threshold for suppression of reconnection with $L_p = d_i$ (Swisdak et al., 2010). Note that small-shear current sheets with $< \sim 90°$ rotation are largely unexplored in this study due to the selection criteria (some have shear angles <90° because we re-calculate the shear angle based on the refined Harris fit time window, which can be different from the time window initially used to detect the magnetic field rotation).

identified current sheets, with or without jets, are thin, having a half-thickness of only a few 100 km or less. We show the half-thickness normalized by the O_2^+ ion inertial length in Figure 8c and by the O_2^+ ion thermal gyroradius in Figure 8d, indicating that the current sheet half-thickness is typically comparable to these ion scale lengths. We also conduct this normalization for O^+ ions, another abundant ion species in the Martian magnetosphere, obtaining similar results. In Figures 8c and 8d, the current sheets with $+V_L$ jets (red solid line) appear to be thicker in the normalized thickness because they tend to be observed in the dayside ionospheric plasma with high densities and low temperatures, leading to small ion inertial lengths and thermal gyroradii. Nevertheless, most of the dayside and nightside current sheets are shown to have a half-thickness smaller than a few ion inertial lengths and thermal gyroradii.

5.5. Dependence on Plasma β and Magnetic Shear

It is proposed that a combination of the magnetic shear and difference of plasma β on the two sides of the current sheet provides another necessary condition for reconnection onset (e.g., Paschmann et al., 2013), based on a theoretical prediction that reconnection will be suppressed by diamagnetic drift of the X-line in small shear current sheets with high β difference (Swisdak et al., 2003, 2010). Consistent trends were identified from observations in the solar wind (Phan et al., 2010; Gosling & Phan, 2013) and at the dayside magnetopause of the Earth (Phan et al., 2013) and Mercury (DiBraccio et al., 2013). Figure 9 shows scatter plots of the magnetic shear and β difference computed from the average magnetic field and total ion β in the precrossing and postcrossing regions for the identified $\pm V_L$ jet events and relatively clean current sheet crossings. The curve denotes a theoretical threshold (Swisdak et al., 2010), below which reconnection should be suppressed. It is seen that most of the identified current sheets, with or without jets, are located above the curve in this parameter space, implying that reconnection will not be inhibited for these current sheets. We note that the identified current sheets are naturally populated in the higher shear, lower β region because of our selection criteria, which require a $> \sim 90°$ magnetic field rotation and the dominance of heavy ions (which is typically the case in the magnetic pileup region, where the magnetic pressure dominates, hence $\beta < 1$). Therefore, our current sheet database is inadequate for testing the theoretical prediction, or rather, Figure 9 demonstrates that relatively large-shear, low-β current sheets (presumably without reconnection suppression) are commonly formed in the near Mars space.

5.6. Summary of Observations

The observed properties of the ion jets within current sheets in the Martian magnetosphere are summarized as follows:

1. Sunward and anti-sunward sub-Alfvénic ion jets accelerated along and within current sheets are widely observed both on the dayside and nightside in the Martian magnetosphere.
2. On average, ion jets are accompanied by the magnetic field configuration and topology consistent with those expected for reconnecting current sheets.
3. We did not find any clear dependence of the jet occurrence on upstream drivers. The ion jets appear to be observed irrespective of the solar wind conditions.
4. Most of the current sheets observed in the Martian magnetosphere (below the ion composition boundary) are thin (~ion inertial lengths and thermal gyroradii) and are embedded in low-β (<1) plasma.

6. Discussion

We first explore alternative explanations for the observed properties of ion jets within current sheets in the Martian magnetosphere. In addition to magnetic reconnection, there are a number of ion acceleration processes that are known to operate in the near Mars space (e.g., Dubinin et al., 2012), including the followings. (i) Field-aligned potential drops of <1 V associated with ambipolar electric fields (Akbari et al., 2019; Xu et al., 2018) cannot explain the observed bidirectional, mostly horizontal flows given the nominal direction of electron pressure gradient. (ii) Field-aligned potential drops of hundreds of volts up to a few kilovolts near cusps and open/closed boundaries of crustal magnetic fields (Brain et al., 2006; Lillis et al., 2018; Lundin et al., 2006; Xu et al., 2020), which are typically accompanied by small magnetic shear generated by field aligned currents, are inconsistent with the large shear current sheets investigated in this paper. (iii) Tailward $\mathbf{J}\times\mathbf{B}$ acceleration up to a keV range by the draped IMF (Dubinin et al., 1993; Dubinin & Fraenz, 2015) cannot account for the sunward ion flows. (iv) The Kelvin-Helmholtz (K-H) instability in the boundary layer between the magnetosheath and ionosphere might produce a locally sunward flow in a fully rolled up vortex, but it cannot explain the sunward flows observed well below the interface between the plasmas of solar wind and ionospheric origins. Besides, it is suggested that K-H vortices could not become fully developed in the near Mars space (Ruhunusiri et al., 2016). (v) Classical ion pickup by motional electric fields in the solar wind and magnetosheath flows cannot explain the sunward flows of dominant heavy ions. At present, we are not aware of any nonreconnection processes that are capable of successfully explaining the properties of the bidirectional ion flows observed within current sheets at Mars as well as the accompanying magnetic field configuration and topology.

We point out that the estimated current sheet thickness of ~1d_i at Mars (Figure 8c) is halfway between electron-scale reconnection without ion coupling (~0.1d_i~ several d_e Phan et al., 2018) and magnetohydrodynamic-scale exhausts with full ion coupling (≥ 10d_i; e.g., Gosling, 2012). At this scale, we can expect partial ion coupling, and simulation results (e.g., Liu et al., 2015; Ma et al., 2018) show that ions are accelerated not fully to 1V_A but partially to a fraction of V_A at a location with the corresponding thickness, which is consistent with the MAVEN observations.

The apparent lack of upstream driver control of the jet occurrence may seem puzzling, given that the Martian magnetosphere is known to be highly dynamic under constant driving by the ever changing solar wind and interplanetary magnetic field (e.g., Halekas et al., 2016). However, the MAVEN observations suggest that sufficiently thin (roughly ion scale) current sheets embedded in low-β plasma are commonly formed in the near Mars space under most upstream conditions (otherwise, significant differences would be seen between the current sheet and overall distributions in Figure 7). This implies that the two known onset conditions for collisionless reconnection (i.e., current sheet thickness and magnetic shear-β difference relationship Paschmann et al., 2013; Swisdak et al., 2010) could be satisfied irrespective of the solar wind conditions. We note that the local absence of a detectable ion jet may not directly represent the absence of magnetic reconnection in the overall current sheet. For example, if the reconnection is patchy and/or intermittent, the chance of spacecraft crossing the spatially and/or temporally confined jets may not be high even if the overall current sheet seems to be capable of reconnection. The spatial and temporal scales of magnetic reconnection at Mars remain elusive given the limitation of single spacecraft measurements.

7. Conclusions and Implications

The extensive survey of ion jets within current sheets in the dayside and nightside magnetosphere of Mars with MAVEN reveals that both of the sunward and anti-sunward jets are widely and commonly observed in the near Mars space. The good agreement between the observed and predicted magnetic field profiles for $\pm V_L$ jet crossings (Figure 6) suggests that the majority of the observed $\pm V_L$ jets are best explained by magnetic reconnection. The relative distributions of magnetic topology (more closed topology for $+V_L$ jets and more draped topology for $-V_L$ jets as seen in Figures 6g and 6h) also support the reconnection scenario. The widespread distributions of jet-containing current sheets in the MSO and geographic coordinates (Figures 3 and 4) imply that magnetic reconnection can take place in a wide range of SZAs, altitudes, and geographic locations within the Martian magnetosphere. Also, the $\pm V_L$ jets are not uncommon. Overall, roughly 10% of the identified clean current sheets exhibit a $+V_L$ or $-V_L$ deviation above our threshold, though we caution that the derived occurrence rate may vary depending on the selection criteria of current sheets and ion jets. Furthermore, most of the identified current sheets appear to satisfy the two known onset conditions for collisionless reconnection, namely current sheet thickness and magnetic shear-β difference relationship, regardless of the solar wind conditions. The common and ubiquitous observations of bidirectional ion jets and of current sheets seemingly capable of reconnection around Mars imply that magnetic reconnection could play an important role in the dynamics of the Martian magnetosphere for most, if not all, of the solar wind conditions in the present epoch.

Data Availability Statement

MAVEN data are publicly available through the Planetary Data System (https://pds-ppi.igpp.ucla.edu).

Acknowledgments
This work was supported by JSPS KAKENHI Grant Number JP19K14784. This work was partially supported by the MAVEN project and the French space agency CNES.

References

Akbari, H., Andersson, L., Peterson, W. K., Espley, J., Benna, M., & Ergun, R. (2019). Ambipolar electric field in the Martian ionosphere: MAVEN measurements. *Journal of Geophysical Research: Space Physics*, *124*, 4518–4524. https://doi.org/10.1029/2018JA026325

Angelopoulos, V., Cruce, P., Drozdov, A., Grimes, E. W., Hatzigeorgiu, N., King, D. A., & Schroeder, P. (2019). The space physics environment data analysis system (SPEDAS). *Space Science Reviews*, *215*(1), 9. https://doi.org/10.1007/s11214-018-0576-4

Artemyev, A. V., Angelopoulos, V., Halekas, J. S., Runov, A., Zelenyi, L. M., & McFadden, J. P. (2017). Mars's magnetotail: Nature's current sheet laboratory. *Journal of Geophysical Research: Space Physics*, *122*, 5404–5417. https://doi.org/10.1002/2017JA024078

Asano, Y., Mukai, T., Hoshino, M., Saito, Y., Hayakawa, H., & Nagai, T. (2003). Evolution of the thin current sheet in a substorm observed by Geotail. *Journal of Geophysical Research*, *108*(A5), 1189. https://doi.org/10.1029/2002JA009785

Baumjohann, W., Roux, A., Le Contel, O., Nakamura, R., Birn, J., Hoshino, M., & Runov, A. (2007). Dynamics of thin current sheets: Cluster observations. *Annales Geophysicae*, *25*(6), 1365–1389.

Beharrell, M. J., & Wild, J. A. (2012). Stationary flux ropes at the southern terminator of Mars. *Journal of Geophysical Research*, *117*, A12212. https://doi.org/10.1029/2012JA017738

Brain, D. A., Baker, A. H., Briggs, J., Eastwood, J. P., Halekas, J. S., & Phan, T. D. (2010). Episodic detachment of Martian crustal magnetic fields leading to bulk atmospheric plasma escape. *Geophysical Research Letters*, *37*, L14108. https://doi.org/10.1029/2010GL043916

Brain, D. A., & Halekas, J. S. (2013). Aurora in Martian mini magnetospheres. *Geophysical Monograph Series*, *197*, 123–132. https://doi.org/10.1029/2011GM001201

Brain, D. A., Halekas, J. S., Peticolas, L. M., Lin, R. P., Luhmann, J. G., Mitchell, D. L., & Reme, H. (2006). On the origin of aurorae on Mars. *Geophysical Research Letters*, *33*, L01201. https://doi.org/10.1029/2005GL024782

Brain, D. A., Lillis, R. J., Mitchell, D. L., Halekas, J. S., & Lin, R. P. (2007). Electron pitch angle distributions as indicators of magnetic field topology near Mars. *Journal of Geophysical Research*, *112*, A09201. https://doi.org/10.1029/2007JA012435

Connerney, J., Espley, J., Lawton, P., Odom, J., Oliversen, R., & Sheppard, D. (2015). The MAVEN magnetic field investigation. *Space Science Reviews*, 257–291. https://doi.org/10.1007/s11214-015-0169-4

Crider, D. H., Brain, D. A., Acuña, M. H., Vignes, D., Mazelle, C., & Bertucci, C. (2004). Mars global surveyor observations of solar wind magnetic field draping around Mars. *Space Science Reviews*, *111*(1), 203–221. https://doi.org/10.1023/B:SPAC.0000032714.66124.4e

DiBraccio, G. A., Dann, J., Espley, J. R., Gruesbeck, J. R., Soobiah, Y., Connerney, J. E. P., & Jakosky, B. M. (2017). MAVEN observations of tail current sheet flapping at Mars. *Journal of Geophysical Research: Space Physics*, *122*, 4308–4324. https://doi.org/10.1002/2016JA023488

DiBraccio, G. A., Espley, J. R., Gruesbeck, J. R., Connerney, J. E. P., Brain, D. A., Halekas, J. S., & Jakosky, B. M. (2015). Magnetotail dynamics at Mars: Initial MAVEN observations. *Geophysical Research Letters*, *42*, 8828–8837. https://doi.org/10.1002/2015GL065248

DiBraccio, G. A., Luhmann, J. G., Curry, S. M., Espley, J. R., Xu, S., Mitchell, D. L., & Jakosky, B. M. (2018). The twisted configuration of the Martian magnetotail: MAVEN observations. *Geophysical Research Letters*, *45*, 4559–4568. https://doi.org/10.1029/2018GL077251

DiBraccio, G. A., Slavin, J. A., Boardsen, S. A., Anderson, B. J., Korth, H., Zurbuchen, T. H., & Solomon, S. C. (2013). MESSENGER observations of magnetopause structure and dynamics at Mercury. *Journal of Geophysical Research: Space Physics*, *118*, 997–1008. https://doi.org/10.1002/jgra.50123

Dubinin, E., & Fraenz, M. (2015). Magnetotails of Mars and Venus. *Geophysical Monograph Series*, *207*, 43–59. https://doi.org/10.1002/9781118842324.ch3

Dubinin, E., Fraenz, M., Fedorov, A., Lundin, R., Edberg, N., Duru, F., & Vaisberg, O. (2012). Ion energization and escape on Mars and Venus. *Space Science Reviews*, *162*, 173–211. https://doi.org/10.1007/978-1-4614-3290-6_6

Dubinin, E., Fraenz, M., Pätzold, M., McFadden, J., Halekas, J. S., DiBraccio, G. A., & Zelenyi, L. (2017). The effect of solar wind variations on the escape of oxygen ions from Mars through different channels: MAVEN observations. *Journal of Geophysical Research: Space Physics*, *122*, 11,285–11,301. https://doi.org/10.1002/2017JA024741

Dubinin, E., Fraenz, M., Woch, J., Zhang, T. L., Wei, J., Fedorov, A., & Lundin, R. (2012). Bursty escape fluxes in plasma sheets of Mars and Venus. *Geophysical Research Letters*, *39*, L01104. https://doi.org/10.1029/2011GL049883

Dubinin, E., Lundin, R., Norberg, O., & Pissarenko, N. (1993). Ion acceleration in the Martian tail: Phobos observations. *Journal of Geophysical Research*, *98*(A3), 3991–3997. https://doi.org/10.1029/92JA02233

Eastwood, J. P., Brain, D. A., Halekas, J. S., Drake, J. F., Phan, T. D., Oieroset, M., & Acuña, M. (2008). Evidence for collisionless magnetic reconnection at Mars. *Geophysical Research Letters*, *35*, L02106. https://doi.org/10.1029/2007GL032289

Espley, J. R. (2018). The Martian magnetosphere: Areas of unsettled terminology. *Journal of Geophysical Research*, *123*, 4521–4525. https://doi.org/10.1029/2018JA025278

Ferguson, B. B., Cain, J. C., Crider, D. H., Brain, D. A., & Harnett, E. M. (2005). External fields on the nightside of Mars at Mars global surveyor mapping altitudes. *Geophysical Research Letters*, *32*, L16105. https://doi.org/10.1029/2004GL021964

Gosling, J. (2012). Magnetic reconnection in the solar wind. *Space Science Reviews*, *172*(1–4), 187–200. https://doi.org/10.1007/s11214-011-9747-2

Gosling, J. T., & Phan, T. D. (2013). Magnetic reconnection in the solar wind at current sheets associated with extremely small field shear angles. *Astrophysical Journal*, *763*(2), 39. https://doi.org/10.1088/2041-8205/763/2/L39

Grigorenko, E. E., Shuvalov, S. D., Malova, H. V., Dubinin, E., Popov, V. Y., Zelenyi, L. M., & McFadden, J. P. (2017). Imprints of quasi-adiabatic ion dynamics on the current sheet structures observed in the Martian magnetotail by MAVEN. *Journal of Geophysical Research: Space Physics*, *122*, 10,176–10,193. https://doi.org/10.1002/2017JA024216

Grigorenko, E. E., Zelenyi, L. M., DiBraccio, G., Ermakov, V. N., Shuvalov, S. D., Malova, H. V., & Dubinin, E. (2019). Thin current sheets of sub-ion scales observed by MAVEN in the Martian magnetotail. *Geophysical Research Letters*, *46*, 6214–6222. https://doi.org/10.1029/2019GL082709

Halekas, J. S., & Brain, D. A. (2010). Global distribution, structure, and solar wind control of low altitude current sheets at Mars. *Icarus*, *206*(1), 64–73. https://doi.org/10.1016/j.icarus.2008.12.032

Halekas, J. S., Eastwood, J. P., Brain, D. A., Phan, T. D., Oieroset, M., & Lin, R. P. (2009). In situ observations of reconnection Hall magnetic fields at Mars: Evidence for ion diffusion region encounters. *Journal of Geophysical Research*, *114*, A11204. https://doi.org/10.1029/2009JA014544

Halekas, J. S., McFadden, J. P., Brain, D. A., Luhmann, J. G., DiBraccio, G. A., Connerney, J. E. P., & Jakosky, B. M. (2018). Structure and variability of the Martian ion composition boundary layer. *Journal of Geophysical Research: Space Physics*, *123*, 8439–8458. https://doi.org/10.1029/2018JA025866

Halekas, J. S., Ruhunusiri, S., Harada, Y., Collinson, G., Mitchell, D. L., Mazelle, C., & Jakosky, B. M. (2016). Structure, dynamics, and seasonal variability of the mars-solar wind interaction: MAVEN solar wind ion analyzer inflight performance and science results. *Journal of Geophysical Research: Space Physics*, *121*, 547–578. https://doi.org/10.1002/2016JA023167

Halekas, J. S., Taylor, E. R., Dalton, G., Johnson, G., Curtis, D. W., McFadden, J. P., & Jakosky, B. M. (2015). The solar wind ion analyzer for MAVEN. *Space Science Reviews*, *195*, 125–151. https://doi.org/10.1007/s11214-013-0029-z

Hara, T., Brain, D. A., Mitchell, D. L., Luhmann, J. G., Seki, K, Hasegawa, H., & Jakosky, B. M. (2016). MAVEN observations of a giant ionospheric flux rope near Mars resulting from interaction between the crustal and interplanetary draped magnetic fields. *Journal of Geophysical Research: Space Physics*, *122*, 828–842. https://doi.org/10.1002/2016JA023347

Hara, T., Harada, Y., Mitchell, D. L., DiBraccio, G. A., Espley, J. R., Brain, D. A., & Jakosky, B. M. (2017). On the origins of magnetic flux ropes in near-Mars magnetotail current sheets. *Geophysical Research Letters*, *44*, 7653–7662. https://doi.org/10.1002/2017GL073754

Hara, T., Seki, K., Hasegawa, H., Brain, D. A., Matsunaga, K., Saito, M. H., & Shiota, D. (2014). Formation processes of flux ropes downstream from Martian crustal magnetic fields inferred from Grad-Shafranov reconstruction. *Journal of Geophysical Research: Space physics*, *119*, 7947–7962. https://doi.org/10.1002/2014JA019943

Harada, Y., Halekas, J. S., DiBraccio, G. A., Xu, S., Espley, J., Mcfadden, J. P., & Jakosky, B. M. (2018). Magnetic reconnection on dayside crustal magnetic fields at Mars: MAVEN observations. *Geophysical Research Letters*, *45*, 4550–4558. https://doi.org/10.1002/2018GL077281

Harada, Y., Halekas, J. S., McFadden, J. P., Espley, J., DiBraccio, G. A., Mitchell, D. L., & Jakosky, B. M. (2017). Survey of magnetic reconnection signatures in the Martian magnetotail with MAVEN. *Journal of Geophysical Research: Space Physics*, *122*, 5114–5131. https://doi.org/10.1002/2017JA023952

Harada, Y., Halekas, J. S., McFadden, J. P., Mitchell, D. L., Connerney, J. E. P., & Jakosky, B. M. (2015a). Marsward and tailward ions in the near-Mars magnetotail: MAVEN observations. *Geophysical Research Letters*, *42*, 8925–8932. https://doi.org/10.1002/2015GL065005

Harada, Y., Halekas, J. S., McFadden, J. P., Mitchell, D. L., Mazelle, C., Connerney, J. E. P., & Jakosky, B. M. (2015b). Magnetic reconnection in the near-Mars magnetotail: MAVEN observations. *Geophysical Research Letters*, *42*, 8838–8845. https://doi.org/10.1002/2015GL065004

Harada, Y., Mitchell, D. L., Halekas, J. S., McFadden, J. P., Mazelle, C., Connerney, J. E. P., & Jakosky, B. M. (2016). MAVEN observations of energy-time dispersed electron signatures in Martian crustal magnetic fields. *Geophysical Research Letters*, *43*, 939–944. https://doi.org/10.1002/2015GL067040

Jakosky, B. M., Lin, R. P., Grebowsky, J. M., Luhmann, J. G., Mitchell, D. F., Beutelschies, G., & Zurek, R. (2015). The Mars atmosphere and volatile evolution (MAVEN) mission. *Space Science Reviews*, *195*, 3–48. https://doi.org/10.1007/s11214-015-0139-x

Kopf, A. J., Gurnett, D. A., DiBraccio, G. A., Morgan, D. D., & Halekas, J. S. (2017). The transient topside layer and associated current sheet in the ionosphere of Mars. *Journal of Geophysical Research*, *122*, 5579–5590. https://doi.org/10.1002/2016JA023591

Kopf, A. J., Gurnett, D. A., Morgan, D. D., & Kirchner, D. L. (2008). Transient layers in the topside ionosphere of Mars. *Geophysical Research Letters*, *35*, L17102. https://doi.org/10.1029/2008GL034948

Krymskii, A. M., Breus, T. K., Ness, N. F., Acuña, M. H., Connerney, J. E. P., Crider, D. H., & Bauer, S. J. (2002). Structure of the magnetic field fluxes connected with crustal magnetization and topside ionosphere at Mars. *Journal of Geophysical Research*, *107*(A9), 1245. https://doi.org/10.1029/2001JA000239

Langlais, B., Thébault, E., Houliez, A., & Lillis, R. J. (2019). A new model of the crustal magnetic field of Mars using MGS and MAVEN. *Journal of Geophysical Research: Planets*, *124*, 1542–1569. https://doi.org/10.1029/2018JE005854

Lillis, R. J., Halekas, J. S., Fillingim, M. O., Poppe, A. R., Collinson, G., Brain, D. A., & Mitchell, D. L. (2018). Field-aligned electrostatic potentials above the Martian exobase from MGS electron reflectometry: Structure and variability. *Journal of Geophysical Research*, *123*, 67–92. https://doi.org/10.1002/2017JE005395

Liu, Y. H., Mouikis, C. G., Kistler, L. M., Wang, S., Roytershteyn, V., & Karimabadi, H. (2015). The heavy ion diffusion region in magnetic reconnection in the Earth's magnetotail. *Journal of Geophysical Research: Space Physics*, *120*, 3535–3551. https://doi.org/10.1002/2015JA020982

Lundin, R. (2011). Ion acceleration and outflow from Mars and Venus: An overview. *Space Science Reviews*, *162*(1–4), 309–334. https://doi.org/10.1007/s11214-011-9811-y

Lundin, R., Winningham, D., Barabash, S., Frahm, R., Holmström, M., Sauvaud, J., & Wurz, P. (2006). Plasma acceleration above Martian magnetic anomalies. *Science*, *311*(5763), 980–983. https://doi.org/10.1126/science.1122071

Ma, Y., Russell, C. T., Toth, G., Chen, Y., Nagy, A. F., & Jakosky, B. M. (2018). Reconnection in the Martian magnetotail: Hall-MHD with embedded particle-in-cell simulations. *Journal of Geophysical Research: Space Physics*, *123*, 3742–3763. https://doi.org/10.1029/2017JA024729

Matsunaga, K., Seki, K., Brain, D. A., Hara, T., Masunaga, K., Mcfadden, J. P., & Jakosky, B. M. (2017). Statistical study of relations between the induced magnetosphere, ion composition, and pressure balance boundaries around Mars based on MAVEN observations. *Journal of Geophysical Research: Space Physics*, *122*, 9723–9737. https://doi.org/10.1002/2017JA024217

McFadden, J. P., Kortmann, O., Curtis, D., Dalton, G., Johnson, G., Abiad, R., & Jakosky, B. (2015). MAVEN SupraThermal and Thermal Ion Compostion (STATIC) Instrument. *Space Science Reviews*, *195*(1–4), 199–256. https://doi.org/10.1007/s11214-015-0175-6

Mitchell, D. L., Mazelle, C., Sauvaud, J. A., Thocaven, J. J., Rouzaud, J., Fedorov, A., & Jakosky, B. M. (2016). The MAVEN solar wind electron analyzer. *Space Science Reviews*, *200*, 495–528. https://doi.org/10.1007/s11214-015-0232-1

Nagai, T., Shinohara, I., Fujimoto, M., Hoshino, M., Saito, Y., Machida, S., & Mukai, T. (2001). Geotail observations of the Hall current system: Evidence of magnetic reconnection in the magnetotail. *Journal of Geophysical Research*, *106*(A11), 25,929–25,949. https://doi.org/10.1029/2001JA900038

Nagy, A., Winterhalter, D., Sauer, K., Cravens, T., Brecht, S., Mazelle, C., & Trotignon, J. (2004). The plasma environment of Mars. *Space Science Reviews*, *111*(1–2), 33–114. https://doi.org/10.1023/B:SPAC.0000032718.47512.92

Øieroset, M., Phan, T., Fujimoto, M., Lin, R., & Lepping, R. (2001). In situ detection of collisionless reconnection in the Earth's magnetotail. *Nature*, *412*(6845), 414–417. https://doi.org/10.1038/35086520

Paschmann, G., Øieroset, M., & Phan, T. (2013). In-situ observations of reconnection in space. *Space Science Reviews*, *178*(2–4), 385–417. https://doi.org/10.1007/s11214-012-9957-2

Paschmann, G., Sonnerup, B. U. Ö., Papamastorakis, I., Sckopke, N., Haerendel, G., Bame, S. J., & Elphic, R. C. (1979). Plasma acceleration at the Earth's magnetopause: Evidence for reconnection. *Nature*, *282*(5736), 243–246. https://doi.org/10.1038/282243a0

Phan, T. D., Eastwood, J. P., Shay, M. A., Drake, J. F., Sonnerup, B. U. O., Fujimoto, M., & Magnes, W. (2018). Electron magnetic reconnection without ion coupling in Earth's turbulent magnetosheath. *Nature*, *557*(7704), 202. https://doi.org/10.1038/s41586-018-0091-5

Phan, T. D., Gosling, J. T., Paschmann, G., Pasma, C., Drake, J. F., Øieroset, M., & Davis, M. S. (2010). The dependence of magnetic reconnection on plasma β and magnetic shear: Evidence from solar wind observations. *Astrophysical Journal-Wikipedia*, *719*(2), L199. https://doi.org/10.1088/2041-8205/719/L199

Phan, T. D., Paschmann, G., Gosling, J. T., Oieroset, M., Fujimoto, M., Drake, J. F., & Angelopoulos, V. (2013). The dependence of magnetic reconnection on plasma β and magnetic shear: Evidence from magnetopause observations. *Geophysical Research Letters*, *40*, 11–16. https://doi.org/10.1029/2012GL054528

Pritchett, P. L. (2001). Geospace environment modeling magnetic reconnection challenge: Simulations with a full particle electromagnetic code. *Journal of Geophysical Research*, *106*(A3), 3783–3798. https://doi.org/10.1029/1999JA001006

Ruhunusiri, S., Halekas, J. S., Espley, J. R., Eparvier, F., Brain, D., Mazelle, C., & Jakosky, B. M. (2018). An artificial neural network for inferring solar wind proxies at Mars. *Geophysical Research Letters*, *45*, 10,855–10,865. https://doi.org/10.1029/2018GL079282

Ruhunusiri, S., Halekas, J. S., McFadden, J. P., Connerney, J. E. P., Espley, J. R., Harada, Y., & Hasegawa, H. (2016). MAVEN observations of partially developed Kelvin-Helmholtz vortices at Mars. *Geophysical Research Letters*, *43*, 4763–4773. https://doi.org/10.1002/2016GL068926

Runov, A., Sergeev, V. A., Baumjohann, W., Nakamura, R., Apatenkov, S., & Rème, H. (2005). Electric current and magnetic field geometry in flapping magnetotail current sheets. *Annales Geophysicae*, *23*(4), 1391–1403. https://doi.org/10.5194/angeo-23-1391-2005

Sonnerup, B. U. Ö., & Cahill, L. J. (1967). Magnetopause structure and attitude from Explorer 12 observations. *Journal of Geophysical Research*, *72*(1), 171–183. https://doi.org/10.1029/JZ072i001p00171

Soobiah, Y. I., Wild, J. A., Beharrell, M. J., Barabash, S., Lillis, R. J., Mitchell, D. L., & Frahm, R. A.Properties of a large-scale flux rope and current sheet region on the dayside of Mars: MGS MAG/ER and MEX ASPERA-3 ELS observations. *Icarus*, *242*, 297–315. https://doi.org/10.1016/j.icarus.2014.08.019

Swisdak, M., Opher, M., Drake, J. F., & Bibi, F. A. (2010). The vector direction of the interstellar magnetic field outside the heliosphere. *Astrophysical Journal*, *710*(2), 1769. https://doi.org/10.1088/0004-637X/710/1769

Swisdak, M., Rogers, B. N., Drake, J. F., & Shay, M. A. (2003). Diamagnetic suppression of component magnetic reconnection at the magnetopause. *Journal of Geophysical Research*, *108*(A5), 1218. https://doi.org/10.1029/2002JA009726

Trotignon, J., Mazelle, C., Bertucci, C., & Acuña, M. (2006). Martian shock and magnetic pile-up boundary positions and shapes determined from the Phobos 2 and Mars Global Surveyor data sets. *Planetary and Space Science*, *54*(4), 357–369. https://doi.org/10.1016/j.pss.2006.01.003

Uluşen, D., & Linscott, I. (2008). Low-energy electron current in the Martian tail due to reconnection of draped interplanetary magnetic field and crustal magnetic fields. *Journal of Geophysical Research*, *113*, E06001. https://doi.org/10.1029/2007JE002916

Vasko, I., Zelenyi, L., Artemyev, A., Petrukovich, A., Malova, H., Zhang, T., & Nakamura, R. (2014). The structure of the Venusian current sheet. *Planetary and Space Science*, *96*(0), 81–89. https://doi.org/10.1016/j.pss.2014.03.013

Weber, T., Brain, D., Mitchell, D., Xu, S., Connerney, J., & Halekas, J. (2017). Characterization of low-altitude nightside Martian magnetic topology using electron pitch angle distributions. *Journal of Geophysical Research: Space Physics*, *122*, 9777–9789. https://doi.org/10.1002/2017JA024491

Weber, T., Mitchell, D., Xu, S., Espley, J., Halekas, J., & Jakosky, B. (2019). The influence of solar wind pressure on Martian crustal magnetic field topology. *Geophysical Research Letters*, *46*(5), 2347–2354. https://doi.org/10.1029/2019GL081913

Xu, S., Fang, X., Mitchell, D. L., Ma, Y., Luhmann, J. G., & Lee, C. O. (2018). Investigation of Martian magnetic topology response to 2017 September ICME. *Geophysical Research Letters*, *45*, 7337–7346. https://doi.org/10.1029/2018GL077708

Xu, S., Liemohn, M. W., Dong, C., Mitchell, D. L., Bougher, S. W., & Ma, Y. (2016). Pressure and ion composition boundaries at Mars. *Journal of Geophysical Research: Space Physics*, *121*, 6417–6429. https://doi.org/10.1002/2016JA022644

Xu, S., Mitchell, D., Liemohn, M., Fang, X., Ma, Y., Luhmann, J., & Jakosky, B. (2017). Martian low-altitude magnetic topology deduced from MAVEN/SWEA observations. *Journal of Geophysical Research: Space Physics*, *122*, 1831–1852. https://doi.org/10.1002/2016JA023467

Xu, S., Mitchell, D., Luhmann, J., Ma, Y., Fang, X., Harada, Y., & DiBraccio, G. A. (2017). High-altitude closed magnetic loops at Mars observed by MAVEN. *Geophysical Research Letters*, *44*, 11,229–11,238. https://doi.org/10.1002/2017GL075831

Xu, S., Mitchell, D. L., McFadden, J. P., Collinson, G., Harada, Y., Lillis, R., & Connerney, J. E. P. (2018). Field-aligned potentials at Mars from MAVEN observations. *Geophysical Research Letters*, *45*, 10,119–10,127. https://doi.org/10.1029/2018GL080136

Xu, S., Mitchell, D. L., McFadden, J. P., Fillingim, M. O., Andersson, L., Brain, D. A., & Espley, J. (2020). Inverted-V electron acceleration events concurring with localized auroral observations at Mars by MAVEN. *Geophysical Research Letters*, *47*, e2020GL087414. https://doi.org/10.1029/2020GL087414

Xu, S., Mitchell, D. L., Weber, T., Brain, D. A., Luhmann, J. G., Dong, C., & Mazelle, C. (2020). Characterizing Mars's magnetotail topology with respect to the upstream interplanetary magnetic fields. *Journal of Geophysical Research: Space Physics*, *125*, e2019JA027755. https://doi.org/10.1029/2019JA027755

Xu, S., Weber, T., Mitchell, D. L., Brain, D. A., DiBraccio, G. A., & Espley, J. (2019). A technique to infer magnetic topology at Mars and its application to the terminator region. *Journal of Geophysical Research: Space Physics*, *124*, 1823–1842. https://doi.org/10.1029/2018JA026366

Yamada, M., Kulsrud, R., & Ji, H. (2010). Magnetic reconnection. *Reviews of Modern Physics*, *82*, 603–664. https://doi.org/10.1103/RevModPhys.82.603